11566 *Inorg. Chem.* **2009**, *48*, 11566–11575
DOI: 10.1021/ic901234d

Inorganic Chemistry
Article

# A Selective Redox and Chromogenic Probe for Hg(II) in Aqueous Environment Based on a Ferrocene−Azaquinoxaline Dyad

**Fabiola Zapata, Antonio Caballero, Arturo Espinosa, Alberto Tárraga,* and Pedro Molina***

*Departamento de Química Orgánica, Facultad de Química, Campus de Espinardo, Universidad de Murcia, E-30100 Murcia, Spain*

Received June 26, 2009

A new chemosensor molecule **4** based on a ferrocene-azaquinoxaline dyad effectively recognizes $Hg^{2+}$ in an aqueous environment as well as $Pb^{2+}$ and $Zn^{2+}$ metal cations in $CH_3CN$ solution through three different channels. Upon recognition, an anodic shift of the ferrocene/ferrocenium oxidation peaks and a progressive red shift ($\Delta\lambda$ = 112−40 nm) of the low energy band, in their absorption spectra, is produced. These changes in the absorption spectra are accompanied by color changes from orange to deep green, for $Hg^{2+}$, and to purple in the cases of $Pb^{2+}$ and $Zn^{2+}$. Remarkably, the redox and colorimetric responses toward $Hg^{2+}$ are preserved in the presence of water ($CH_3CN/H_2O$, 3/7). The emission spectrum of **4** in $CH_3CN$ ($\lambda_{exc}$ = 270 nm) undergoes important chelation enhancement of fluorescence (CHEF) in the presence of $Hg^{2+}$ (CHEF = 204), $Pb^{2+}$ (CHEF = 90), and $Zn^{2+}$ (CHEF = 184) metal cations. Along with the spectroscopic data, the combined $^1H$ NMR data of the complexes and the theoretical calculation suggest the proposed bridging coordination modes.

## Introduction

The development of selective and sensitive imaging tools capable of monitoring heavy- and transition-metal ions has attracted considerable attention because of the wide use of these metal ions and their subsequent impact on the environment and nature.[1] The $Hg^{2+}$ ion is considered a highly toxic element, and its contamination is a global problem. A major source of human exposure stems from a variety of natural and anthropogenic sources[2] including oceanic and volcanic emission,[3] gold mining[4] solid waste incineration, and combustion of fossil fuel.[5] Exposure of mercury even at low concentration leads to digestive, kidney, and especially neurological diseases.[6] Although the pollutant character of mercury has mainly been focused on the occurrence of methylmercury in the marine food chain, the mercury problem is not limited to the aquatic food chain since rice has recently been proposed as the major source for methylmercury intake from food in parts of the Chinese population, and the results indicate that this derivative is more prominent in the rice grains than would be expected from the occurrence of methylmerucry versus inorganic mercury in the soil.[7] Due to the potential for mercury exposure in day to day life, the development of techniques for mercury hazard assesment and mercury pollution management has drawn worldwide attention.[8] Therefore, many laboratories have focused on "colorimetric",[9] redox active,[10] and/or fluorescent[11] highly selective mercury-responsive small-molecule chemosensors.

*To whom correspondence should be addressed. E-mail: pmolina@um.es (P.M.); atarraga@um.es (A.T.).

(1) (a) *Fluorescent Chemosensors for Ion and Molecule Recognition*; Czarnik, A. W., Ed.; American Chemical Society: Washington, DC, 1993; p 1. (b) de Silva, A. P.; Gunaratne, H. Q. N.; Gunnlaugsson, T.; Huxley, A. J. M.; McCoy, C. P.; Rademacher, J. T.; Rice, T. E. *Chem. Rev.* **1997**, *97*, 1515–1566.
(2) Benoit, J. M.; Fitzgerald, W. F.; Damman, A. W. *Environ. Res.* **1998**, *78*, 118–133.
(3) Renzoni, A.; Zino, F.; Franchi, E. *Environ. Res.* **1998**, *77*, 68–72.
(4) Malm, O. *Environ. Res.* **1998**, *77*, 73–78.
(5) Mercury Update: Impact on Fish Advisories. EPA Fact Sheet EPA-823-F-01-011; EPA; Office of Water: Washington, DC, 2001.
(6) (a) Grandjean, P.; Weihe, P.; White, R. F.; Debes, F. *Environ. Res.* **1998**, *77*, 165–172. (b) Boening, D. W. *Chemosphere* **2000**, *40*, 1335–1351. (c) Harris, H. H.; Pickering, I. J.; George, G. N. *Science* **2003**, *301*, 1203–1203.
(7) (a) Feng, X. B.; Li, P.; Qiu, G. L.; Wang, S.; Li, G. H.; Shang, L. H.; Meng, B.; Jiang, H. M.; Bai, W. Y.; Li, Z. G.; Fu, X. W. *Environ. Sci. Technol.* **2008**, *42*, 326–332. (b) Krupp, E. M.; Mestrot, A.; Wielgus, J.; Meharg, A. A.; Feldmann, J. *Chem. Commun.* **2009**, 4257−4259.
(8) Nolan, E. M.; Lippard, S. *J. Chem. Rev.* **2008**, *108*, 3443–3480. Molina, P.; Tárraga, A.; Caballero, A. *Eur. J. Inorg. Chem.* **2008**, 4301–4317.
(9) (a) Brummer, O.; La Clair, J. J.; Janda, K. D. *Org. Lett.* **1999**, *1*, 415–418. (b) Choi, M. J.; Kim, M. Y.; Chang, S. K. *Chem. Commun.* **2001**, 1664–1665. (c) Zhao, Y.; Zhong, Z. Q. *Org. Lett.* **2006**, *8*, 4715–4717. (d) Tatay, S.; Gaviña, P.; Coronado, E.; Palomares, E. *Org. Lett.* **2006**, *8*, 3857–3860. (e) Zhao, Y.; Zhong, Z. Q. *J. Am. Chem. Soc.* **2006**, *128*, 9988–9989. (f) Nazeeruddin, M. K.; Di Censo, D.; Humphry-Baker, R.; Grätzel, M. *Adv. Funct. Mater.* **2006**, *16*, 189–194. (g) Coronado, E; Galán-Mascarós, J. R.; Martí-Gastaldo, C.; Palomares, E.; Durrant, J. R.; Vilar, R.; Grätzel, M.; Nazeeruddin, M. K. *J. Am. Chem. Soc.* **2005**, *127*, 12351–12356. (h) Balaji, T.; El-Safty, S. A.; Matsunaga, H.; Hanaoka, T.; Mizukami, F. *Angew. Chem., Int. Ed.* **2006**, *45*, 7202–7208. (i) Lin, S. Y.; Wu, S. M.; Chen, C. H. *Angew. Chem., Int. Ed.* **2006**, *45*, 4948–4951. (j) Diez-Gil, C.; Caballero, A.; Ratera, I.; Tárraga, A.; Molina, P.; Veciana, J. *Sensors* **2007**, *7*, 3481–3488.
(10) (a) Jiménez, D.; Martínez-Máñez, R.; Sancenón, F.; Soto, J. *Tetrahedron Lett.* **2004**, *45*, 1257–1259. (b) Caballero, A.; Lloveras, V.; Curiel, D.; Tárraga, A.; Espinosa, A.; García, R.; Vidal-Gancedo, J.; Rovira, C.; Wurst, K.; Molina, P.; Veciana, J. *Inorg. Chem.* **2007**, *46*, 825–838.

 Published on Web 11/19/2009 

Among heavy metals, lead is the most abundant, ranks second in the list of toxic substances, and is often encountered due to its wide distribution in the environment as well as its current and previous use in batteries, gasoline, and pigments. Lead pollution is an ongoing danger to human health, particularly in children (memory loss, irritability, anemia, muscle paralysis, and mental retardation),[12] and the environment, as most of the 300 million tons of this heavy metal mined to date are still circulating in soil and groundwater.[13] Despite efforts to reduce global emissions, lead poisoning remains the world's most common environmentally caused disease.[14] Thus, the level of this detrimental ion, which is present in tap water as a result of dissolution from household plumbing systems, is the object of several official norms. The World Health Organization established in 1996 a guideline for drinking-water quality,[15] which included a lead maximal value of 10 $\mu$g $L^{-1}$. Thus, in regulating the levels of $Pb^{2+}$, the detection and monitoring of this metal cation by methods which allow the development of selective and sensitive assays becomes very important. As many heavy metals are known as fluorescence quenchers via enhanced spin−orbital coupling,[16] energy or electron transfer,[17] development of fluorescent sensors for $Pb^{2+}$ presents a challenge. In this context, considerable efforts have been undertaken to develop fluorescent chemosensors for $Pb^{2+}$ ions based on peptide,[18] protein,[19]DNAzyme,[20] polymer,[21] and small-molecule[22] scaffolds. There is, however, a paucity of use of multichannel receptors as potential guest reporters via multiple signaling patterns.[23] Specifically, as we report here, the development of multichannel (chromogenic/fluorogenic/electrochemical) $Pb^{2+}$ selective chemosensors is, as far as we know, an unexplored subject,[23e,24] and only three dual chromogenic and redox receptors have been recently described.[25]

Zinc is the second most abundant transition metal following iron and a fundamental element in natural biological systems.[26] Zinc is an essential nutrient required for normal growth and development[27] and for key cellular processes such as DNA repair[28] and apoptosis.[29]

Currently, there is a high demand for systems able to sense the $Zn^{2+}$ cation, which is spectroscopically silent because of its $3d^{10}4s^0$ electronic configuration. Moreover, it is still a challenge to develop simple chemosensors that can discriminate $Zn^{2+}$ from $Cd^{2+}$ because cadmium and zinc are in the same group of the periodic table and have similar properties, usually causing similar spectral changes after interactions with chemosensors.[30]

Pyrido[2,3-*b*]pyrazines also named 5-azaquinoxalines or 1,4,5-triazanaphthalenes have remarkable applications in the field of electroconductive and dipolar electroluminiscent devices with tunable emission characteristics.[31]

(11) (a) Caballero, A.; Martínez, R.; Lloveras, V.; Ratera, I.; Vidal-Gancedo, J.; Wurst, K.; Tárraga, A.; Molina, P.; Veciana, J. *J. Am. Chem. Soc*. **2005**, *127*, 15666–15667. (b) Nolan, E. M; Lippard, S. J. *J. Am. Chem. Soc*. **2003**, *125*, 14270–14271. (c) Ros-Lis, J. V.; Marcos, M. D.; Martínez-Máñez, R.; Rurack, K.; Soto, J. *Angew. Chem., Int. Ed*. **2005**, *44*, 4405–4407. (d) Aragoni, M. C.; Arca, M.; Bencini, A.; Blake, A. J.; Caltagirone, C.; Decortes, A.; Demartin, F.; Devillanova, F. A.; Faggi, E.; Doci, L. S.; Garau, A.; Isaia, F.; Lippolis, V.; Prodi, L.; Wilson, C.; Valtancoli, B.; Zaccheroni, N. *Dalton Trans*. **2005**, 2994–3004. (e) Shamsipur, M.; Hosseini, M.; Alizadeh, K.; Alizadeh, N.; Yari, A.; Caltagirone, C.; Lippolis, V. *Anal. Chim. Acta* **2005**, *533*, 17–24. (f) Kim, I. B.; Bunz, U. H. F. *J. Am. Chem. Soc*. **2006**, *128*, 2818–2819. (g) Kim, I. B.; Erdogan, B.; Wilson, J. N.; Bunz, U. H. F. *Chem.—Eur. J*. **2004**, *10*, 6247–6254. (h) Ou, S. J.; Lin, Z. H.; Duan, C. Y.; Zhang, H. T.; Bai, Z. P. *Chem. Commun*. **2006**, 4392–4394. (i) Wang, J. B.; Qian, H. *Org. Lett*. **2006**, *8*, 3721–3724. (j) Martínez, R.; Zapata, F.; Caballero, A.; Espinosa, A.; Tárraga, A.; Molina, P. *Org. Lett*. **2006**, *8*, 3235–3238. (k) Ono, A.; Togashi, H. *Angew. Chem., Int. Ed*. **2004**, *43*, 4300–4302. (l) Yoon, S.; Albers, A. E.; Wong, A. P.; Chang, C. J. *J. Am. Chem. Soc*. **2005**, *127*, 16030–16031. (m) Zhu, X. J.; Fu, S. T.; Wong, W. K.; Guo, H. P.; Wong, W. Y. *Angew. Chem., Int. Ed*. **2006**, *45*, 3150–3154. (n) Diez-Gil, C.; Martinez, R.; Ratera, I.; Tárraga, A.; Molina, P.; Veciana, J. *J. Mater. Chem*. **2008**, *18*, 1997–2002. (o) Yuan, M.; Zhou, W.; Liu, X.; Zhu, M.; Li, J.; Yin, X.; Zheng, H.; Zuo, Z.; Ouyang, C.; Liu, H.; Li, Y.; Zhu, D. *J. Org. Chem*. **2008**, *73*, 5008–5014. (p) Wu, D.; Huang, W.; Lin, Z.; Duan, C.; He, C.; Wu, S.; Wang, D. *Inorg. Chem*. **2008**, *47*, 7190–7201. (q) Huang, W.; Song, C.; He, C.; Lv, G.; Hu, X.; Zhu, X.; Duan, C. *Inorg. Chem*. **2009**, *48*, 5061–5072.

(12) Lin-Fu, J. S. Lead Poisoning, A Century of Discovery and Rediscovery. In *Human Lead Exposure*; Needleman, H. L., Ed.; Lewis Publishing: Boca Raton, FL, 1992.

(13) Flegal, A. R.; Smith, D. R. *Environ. Res*. **1992**, *58*, 125–133.

(14) Claudio, E. S.; Godwin, H. A.; Magyar, J. S. *Prog. Inorg. Chem*. **2003**, *51*, 1−144 and references therein.

(15) World Health Organization, Guidelines for drinking-water quality, Geneva, 2nd ed., 1996; Vol. *2*, p 940.

(16) McClure, D. S. *J. Chem. Phys*. **1952**, *20*, 682–686.

(17) Varnes, A. W.; Dodson, R. B.; Whery, E. L. *J. Am. Chem. Soc*. **1972**, *94*, 946–950.

(18) Deo, S.; Godwin, H. A. *J. Am. Chem. Soc*. **2000**, *122*, 174–175.

(19) Chen, P.; Greenberg, B.; Taghvi, S.; Romano, C.; van der Lelie, D.; He, C. *Angew. Chem., Int. Ed*. **2005**, *44*, 2715–2719.

(20) (a) Liu, J.; Lu, Y. *J. Am. Chem. Soc*. **2000**, *122*, 10466–10467. (b) Liu, J.; Lu, Y. *J. Am. Chem. Soc*. **2003**, *125*, 6642–6643. (c) Liu, J.; Lu, Y. *J. Am. Chem. Soc*. **2004**, *126*, 12298–12305. (d) Chang, I. H.; Tulock, J. J.; Liu, J.; Kim, W.-S.; Cannon, D. M., Jr.; Lu, Y.; Bohn, P. W.; Sweedler, J. V.; Cropek, D. M. *Environ. Sci. Technol*. **2005**, *39*, 3756–376.

(21) Kim, I.-K.; Dunkhorst, A.; Gilbert, J.; Bunz, U. H. F. *Macromolecules* **2005**, *38*, 4560–4562.

(22) (a) Kwon, J. Y.; Jang, Y. J.; Lee, Y. J.; Kim, K. M.; Seo, M. S.; Nam, W.; Yoon, J. *J. Am. Chem. Soc*. **2005**, *127*, 10107–10111. (b) Kavallieratos, K.; Rosenberg, J. M.; Chen, W.-Z.; Ren, T. *J. Am. Chem. Soc*. **2005**, *127*, 6514–6515. (c) Lee, J. Y.; Kim, S. K.; Jung, J. H.; Kim, J. S. *J. Org. Chem*. **2005**, *70*, 1463–1466. (d) Liu, J.-M.; Bu, J-H; Zheng, Q.-Y.; Chen, C.-F.; Huang, Z.-T. *Tetrahedron Lett*. **2006**, *47*, 1905–1908. (e) Metivier, R.; Leray, I.; Valeur, B. *Chem. Commun*. **2003**, 996–997. (f) Metivier, R.; Leray, I.; Valeur, B. *Chem.—Eur. J*. **2004**, *10*, 4480–4490. (g) Chen, C.-T.; Huang, W.-P. *J. Am. Chem. Soc*. **2002**, *124*, 6246–6247. (h) Ma, L.-J.; Liu, Y.-F.; Wu, Y. *Chem. Commun*. **2006**, 2702–2704. (i) Wu, F.-Y.; Bae, S. W.; Hong, J.-I. *Tetrahedron Lett*. **2006**, *47*, 851–8854. (j) He, Q.; Miller, E. W.; Wong, A. P.; Chang, C. J. *J. Am. Chem. Soc*. **2006**, *128*, 9316–9317. (k) Crego-Calama, M.; Reinhoudt, D. N. *Adv. Mater*. **2001**, *13*, 1171–1174. (l) Lee, J. Y.; Kim, S. K.; Jung, J. H.; Kim, J. S. *J. Org. Chem*. **2005**, *70*, 1463–1466.

(23) (a) Jiménez, D.; Martínez-Mañez, R.; Sancenón, F.; Ros-Lis, J. V.; Soto, J.; Benito, A.; García-Breijo, E. *Eur. J. Inorg. Chem*. **2005**, 2393–2403. (b) Descalzo, A. B.; Rurack, K.; Weisshoff, H.; Martínez-Mañez, R.; Marcos, M. D.; Amorós, P.; Hoffmann, K.; Soto, J. *J. Am. Chem. Soc*. **2005**, *127*, 184–200. (c) Martínez-Mañez, R.; Sancenón, F. *Coord. Chem. Rev*. **2006**, *250*, 3081–3093. (d) Romero, T.; Caballero, A.; Espinosa, A.; Tárraga, A.; Molina, P. *Dalton Trans*. **2009**, 2121–2129. (e) Zapata, F.; Caballero, A.; Espinosa, A.; Tárraga, A.; Molina, P. *J. Org. Chem*. **2009**, *74*, 4787–4796. (f) Romero, T.; Caballero, A.; Tárraga, A.; Molina, P. *Org. Lett*. **2009**, *11*, 3466–3469.

(24) Zapata, F.; Caballero, A.; Espinosa, A.; Tárraga, A.; Molina, P. *Org. Lett*. **2008**, *10*, 41–44.

(25) (a) Xue, H.; Tang, X.-J.; Wu, L.-Z.; Zhang, L.-P.; Tung, C.-H. *J. Org. Chem*. **2005**, *70*, 9727–9734. (b) Remeter, D.; Blanchard, P.; Allain, M.; Grosu, I.; Roncali, J. *J. Org. Chem*. **2007**, *72*, 5285–5290. (c) Caballero, A.; Espinosa, A.; Tárraga, A.; Molina, P. *J. Org. Chem*. **2008**, *73*, 5489–5497.

(26) (a) J. J. R. F.de Silva, Williams, R. J. P. Zinc: Lewis Acid Catalysis and Regulation. *The Biological Chemistry of Elements: The Inorganic Chemistry of Life*, 2nd ed.; Oxford University Press: New York, 2001. (b) Williams, R. J. P.; da Silva, J. J. R. F. *Coord. Chem. Rev*. **2000**, *200−202*, 247–348.

(27) Vallee, B. L.; Falchuk, K. H. *Physiol. Rev*. **1993**, *73*, 79–118.

(28) (a) Ho, E.; Ames, B. N. *Proc. Natl. Acad. Sci. U.S.A*. **2002**, *99*, 16770–16775. (b) Daiyasu, H.; Osaka, K.; Ishino, Y.; Toh, H. *FEBS Lett*. **2001**, *503*, 1–6.

(29) Troung-Tran, A. Q.; Carter, J.; Ruffin, R. E.; Zalewski, P. D. *Biometals* **2001**, *14*, 315–330.

(30) *Interalia*; see: (a) Zapata, F.; Caballero, A.; Espinosa, A.; Tárraga, A.; Molina, P. *Org. Lett*. **2007**, *9*, 2385–2388. (b) Sreejitch, S.; Divya, K. P.; Ajayaghosh, A. *Chem. Commun*. **2008**, 2903–2905. (c) Mikata, Y.; Yamashita, A.; Kawamura, A.; Kouno, H.; Miyamoto, Y.; Tamotsu, S. *Dalton Trans*. **2009**, 3800–3806. (d) Nolan, E. N.; Lippard, S. J. *Acc. Chem. Res*. **2009**, *42*, 193–203.

(31) (a) Lukes, V.; Breza, M.; Vega, D.; Hrdlovic, P.; Krajeovic, J.; Laurinc, V. *Synth. Met*. **2001**, *124*, 279–286. (b) Justin Thomas, K. R.; Lin, J. T.; Tao, Y.-T.; Chuen, C. H. *J. Mater. Chem*. **2002**, *12*, 3516–3522.

Diverse bonding modes of the pyrido[2,3-*b*]pyrazine unit ranging from monodentate through any of the three nitrogen atoms, bidentate through either the two nitrogen atoms of the pyrazine ring or the pyridine and pyrazine nitrogen atoms on opposite sides of the molecule, to short-bite nitrogen ligand (exobidentate ligand) by using pyridine and pyrazine nitrogen atoms on the same side of the molecule are observed.[32] The identity of the metal ions dictate the topology of the complex.

Fluxional behavior associated with the coordination ambiguity of the 1,4,5-triazanaphthalene has been studied by high-resolution $^1$H NMR spectroscopy. In a mononuclear complex of 1,4,5-triazanaphthalene, competition between the more basic pyridine and the better $\pi$ backdonating pyrazine nitrogen centers leads to various positions for the nondegenerate equilibria between linkage isomers.[33] The nitrogen atom of the pyridine ring seems to be also the preferential site of quaternization, and this process causes an increase in the vecinal coupling constant between H-α and H-$\beta$ and broadening of the H-α proton signals in the $^1$H NMR spectra.[34]

Despite their easy synthesis and coordination properties, pyrido[2,3-*b*]pyrazines have never been used for sensing purposes to the best of our knowledge. We have embarked upon designing ferrocene-based systems that can sense anions and metal ions.[25c,35] Recently, we have found that a number of ferrocene−azaheterocycle dyads selectively sense transition metal cations thorough several channels.[10b,23d,24] In this context, 2,3-bis(ferrocenyl) pyrido[2,3-*b*]pyrazine **4** has been chosen to develop a multichannel system, where the chromogenic and fluorescent reporters are integrated with and the redox unit is linked to the guest cation binding site.

## Experimental Section

**General Methods.** All reactions were carried out under $N_2$ and using solvents which were dried according to routine procedures. Column chromatography was performed with the use of a column of dimensions 60 cm × 4.5 cm and of silica gel (60 A C.C. 70−200 $\mu$m, sds) as the stationary phase. NMR spectra were recorded at 200, 300, and 400 MHz. The following abbreviations for stating the multiplicity of the signals in the NMR spectra were used: s (singlet), st (pseudotriplet), dd (double doublet), m (multiplet), q (quaternary carbon). The ESI mass spectra were recorded on an AGILENT V spectrometer. Elemental analyses were carried out on a Carlo-Erba EA-1108 analyzer. CV and OSWV voltammetries were performed with a conventional three-electrode configuration consisting of platinum working and auxiliary electrodes and an SCE reference electrode. The experiments were carried out with a $10^{-3}$ M solution of sample in $CH_3CN$ or $CH_3CN/H_2O$ (3/7) containing 0.1 M $(n\text{-}C_4H_9)_4NPF_6$ (TBAHP) as supporting electrolyte. All of the potential values reported are relative to the decamethylferrocene (DMFc) couple at room temperature. Deoxygenation of the solutions was achieved by bubbling nitrogen for at least 10 min, and the working electrode was cleaned after each run. The cyclic voltammograms were recorded with a scan rate increasing from 0.05 to 1.00 V s$^{-1}$, while the Osteryoung square wave voltammograms were recorded at a scan rate of 0.1 V s$^{-1}$ with a pulse height of 25 mV and a step time of 50 ms. Typically, the receptor ($1 \times 10^{-3}$ mol) was dissolved in solvent (5 mL) and TBAHP (base electrolyte) (0.193 g) was added. The guest under investigation was then added as a $2.5 \times 10^{-2}$ M solution in $CH_3CN$ using a microsyringe, while the cyclic voltammetric properties of the solution were monitored. DMFc was used either as an external or internal reference both for potential calibration and for reversibility criteria. Under similar conditions the ferrocene has $E^\circ = -0.077$ V vs SCE and the anodic peak−cathodic peak separation is 67 mV. UV−vis and fluorescence spectra were carried out in $CH_3CN$ or $CH_3CN/H_2O$ (3/7) solutions at $c = 1 \times 10^{-4}$ M and $c \approx 10^{-5}$ M, respectively, as it is stated in the corresponding figure captions.

**Computational Details.** Calculated geometries were fully optimized in the gas phase with tight convergence criteria at the DFT level with the Gaussian 03 package,[36] using the hybrid meta functional mPW1B95[37] that has been recommended for general purpose applications and was developed to produce a better performance where weak interactions are involved, such as those between ligands and heavy metals.[38] The 6-31G** basis set was used for all atoms, adding diffuse functions on donor atoms (N and O) (denoted as aug6-31G**) as well as the Lanl2DZ basis set with an effective core potential (Lanl2DZecp) for Zn, Hg, and Pb. Ultrafine grids (99 radial shells and 590 angular points per shell) were employed for numerical integrations. From these gas-phase optimized geometries, all reported data were obtained by means of single-point (SP) calculations, at the same level of theory unless otherwise stated. Bond orders were characterized by the Wiberg bond index (WBI)[39] and calculated with the Natural Bond Orbital (NBO) population analysis, as the sum of squares of the off-diagonal density matrix elements between atoms. The topological analysis of the electronic charge density was conducted by means of the Bader AIM (Atoms-In-Molecules)[40] methodology using the AIM2000 software.[41] Energy values are uncorrected for the zero-point vibrational energy and were computed at the aug6-311G**/Lanl2DZecp level, considering solvent (acetonitrile) effects by using the Cossi and Barone

(32) (a) Tresoldi, G.; Lo Schiavo, S. L.; Nicolo, F.; Cardiano, P.; Piraino, P. *Inorg. Chim. Acta* **2003**, *344*, 190–196. (b) Stoklosa, H. J.; Wasson, J. R.; Brown, E. V.; Richardson, H. W.; Hatfield, W. E. *Inorg. Chem.* **1975**, *14*, 2378–2382. (c) Manson, J. L. *Inorg. Chem.* **2003**, *42*, 2602–2605. (d) Ghosh, T.; Maiya, B. G.; Samanta, A. *Dalton Trans.* **2006**, 795–801.

(33) Bessenbacher, C.; Kaim, W. *J. Organomet. Chem.* **1989**, *369*, 83–103.

(34) Chupakhin, O. N.; Charushin, V. N.; Chernyshev, A. I.; Esipov, S. E. *Magn. Reson. Chem.* **1985**, *23*, 437–441.

(35) Zapata, F.; Caballero, A.; Espinosa, A.; Tárraga, A.; Molina, P. *J. Org. Chem.* **2008**, *73*, 4034–4044.

(36) Frisch, M. J.; Trucks, G. W.; Schlegel, H. B.; Scuseria, G. E.; Robb, M. A.; Cheeseman, J. R.; Montgomery, Jr., J. A.; Vreven, T.; Kudin, K. N.; Burant, J. C.; Millam, J. M.; Iyengar, S. S.; Tomasi, J.; Barone, V.; Mennucci, B.; Cossi, M.; Scalmani, G.; Rega, N.; Petersson, G. A.; Nakatsuji, H.; Hada, M.; Ehara, M.; Toyota, K.; Fukuda, R.; Hasegawa, J.; Ishida, M.; Nakajima, T.; Honda, Y.; Kitao, O.; Nakai, H.; Klene, M.; Li, X.; Knox, J. E.; Hratchian, H. P.; Cross, J. B.; Bakken, V.; Adamo, C.; Jaramillo, J.; Gomperts, R.; Stratmann, R. E.; Yazyev, O.; Austin, A. J.; Cammi, R.; Pomelli, C.; Ochterski, J. W.; Ayala, P. Y.; Morokuma, K.; Voth, G. A.; Salvador, P.; Dannenberg, J. J.; Zakrzewski, V. G.; Dapprich, S.; Daniels, A. D.; Strain, M. C.; Farkas, O.; Malick, D. K.; Rabuck, A. D.; Raghavachari, K.; Foresman, J. B.; Ortiz, J. V.; Cui, Q.; Baboul, A. G.; Clifford, S.; Cioslowski, J.; Stefanov, B. B.; Liu, G.; Liashenko, A.; Piskorz, P.; Komaromi, I.; Martin, R. L.; Fox, D. J.; Keith, T.; Al-Laham, M. A.; Peng, C. Y.; Nanayakkara, A.; Challacombe, M.; Gill, P. M. W.; Johnson, B.; Chen, W.; Wong, M. W.; Gonzalez, C.;Pople, J. A.; *Gaussian 03*, revision B.03; Gaussian, Inc.: Wallingford, CT, 2004.

(37) (a) Zhao, Y.; Truhlar, D. G. *J. Phys. Chem. A* **2004**, *108*, 6908–6918. (b) Zhao, Y.; Truhlar, D. G. *J. Phys. Chem. A* **2005**, *109*, 5656–5667.

(38) For instance, see: Muñiz, J.; Sansores, L. E.; Martínez, A.; Salcedo, R. *J. Mol. Struct.* **2007**, *820*, 141–147.

(39) Wiberg, K. *Tetrahedron* **1968**, *24*, 1083–1096.

(40) Bader, R. F. W. *Atoms in Molecules: A Quantum Theory*; Oxford University Press: Oxford, 1990.

(41) (a) AIM2000 v. 2.0, designed by Biegler-König, F. W. and Schönbohm, J. **2002**. Home page http://www.aim2000.de/.Biegler-König, F.; Schönbohm, J.; Bayles, D. *J. Comput. Chem.* **2001**, *22*, 545–559. (b) Biegler-König, F.; Schönbohm, J. *J. Comput. Chem.* **2002**, *23*, 1489–1494.

CPCM (conductor-like polarizable continuum model) modification[42] of Tomasi's PCM formalism[43] and correcting the basis set superposition error (BSSE) by means of the Bq-approach at the optimization level. Energy values are not given for larger complexes having 2:1 or 2:2 ligand/metal stoichometries due to systematic convergence problems on BSSE evaluation

**Improved Procedure for the Preparation of Diferrocenylethane-1,2-dione, 3.** To a solution of ferrocene (5 g, 26 mmol) in dry diethyl ether (60 mL), *n*-BuLi (1.6 M in *n*-hexane) (35.3 mL, 56 mmol) was added dropwise, under a nitrogen atmosphere. Once such addition was finished, tetramethylendiamine (TMEDA) (8.5 mL, mmol) was slowly added and the reaction mixture was stirred at room temperature for 20 h. Subsequently, this solution was transferred dropwise, by cannula and under nitrogen, to a THF solution (50 mL) of 1,4-dimethylpyperazine-2,3-dione (1.2 g, 8.5 mmol), and the reaction mixture was stirred at room temperature for 5 min. The solvent was removed under reduced pressure, and the resulting crude product was dissolved in $CH_2Cl_2$ (400 mL). After extraction with $H_2O$ (3 × 100 mL), the combined organic layers were dried over anhydrous $Na_2SO_4$. The solvent was removed under vacuum, and the product was purified by column chromatography, using $CH_2Cl_2$ as eluent, to yield 1.2 g (21%) of **3** as a red-purple solid, 192−194 °C (lit[44] mp 193.5−195.5 °C), whose characterization data ($^1$H NMR, $^{13}$C NMR, and MS) are identical to those previously reported.

**Synthesis of 2,3-Diferrocenylpyrido[2,3-*b*]pyrazine, 4.** 2,3-Diaminopyridine (77 mg, 0.7 mmol) was added to a solution of diferrocenylethane-1,2-dione **3** (0.3 g, 0.7 mmol) in ethanol (50 mL). The mixture was stirred under reflux temperature for 7 days during which time a purple solid precipitated, which was isolated by filtration, washed with cold diethyl ether (3 × 10 mL), dried in vacuum, and crystallized from $CH_2Cl_2$/diethyl ether (1/1). Yield, 80%. Mp 260 °C (d). $^1$H NMR ($CDCl_3$): $\delta$ 4.04 (s, 5H), 4.08 (s, 5H), 4.35 (m, 4H), 4.68 (st, 2H), 4.77 (st, 2H), 7.59 (dd, 1H, $J$ = 8.1 Hz, $J$ = 4.2 Hz), 8.35 (dd, 1H, $J$ = 1.8 Hz, $J$ = 8.1 Hz), 9.05 (dd, 1H, $J$ = 1.8 Hz, $J$ = 4.2 Hz). $^{13}$C NMR ($CDCl_3$): $\delta$ 68.9 (2×CH), 69.7 (2×CH), 69.9 (5×CH), 70.0 (5×CH), 71.7 (2×CH), 71.8 (2×CH), 82.8 (2×q), 85.1 (2×q), 123.9 (CH), 135.0 (q), 137.2 (CH), 152.9 (CH), 154.3 (q), 157.3 (2×q). ES MS, $m/z$ (relative intensity): 499 ($M^+$, 100). Anal. Calcd for $C_{27}H_{21}Fe_2N_3$: C, 64.97; H, 4.24; N, 8.42. Found: C, 64.72; H, 4.40; N, 8.16.

## Results and Discussion

**Synthesis.** Receptor **4** was prepared by the following two-step sequence (Scheme 1): (a) reaction of 1,1′-dilithioferrocene **1** with the readily available 1,4-dimethylpiperazine-2,3-dione **2** to give diferrocenylethane-1,2-dione **3** in 21% yield and (b) condensation of the dicarbonyl compound **3** with 2,3-diaminopyridine to give the receptor **4** in 80% yield. Although the conversion of **2** → **3** has already been described by using ferrocenyllithium as a metalating agent,[45] we have observed that 1,1′-dilithioferrocene gave rise to compound **3** more easily and in a much better yield. Probably the difficulties encountered following the tedious reported procedure could be associated to the use of *t*-BuLi and to the periods needed to achieve not only the minimum proportion of unreacted ferrocene but also the maximum ratio between the monometalated and dimetalated species. The 1,1′-dimetalated ferrocene **1** was prepared by lithiation of the metallocene unit employing butyllithium-TMEDA. The optimum conditions for the dilithiation process utilized a slightly greater than 2:1 molar ratio of *n*-BuLi and diamine to ferrocene and a reaction period of 20 h, the reaction being run at room temperature.[47]

**Scheme 1.** Preparation of Receptor **4**[a]

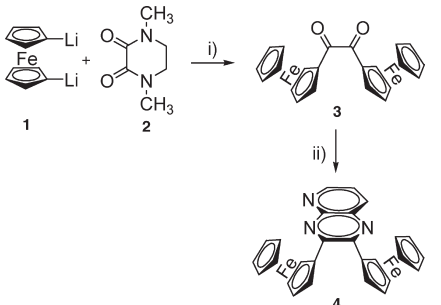


[a] (i) rt, 5 min; (ii) 2,3-diaminopyridine, EtOH, reflux, 7 days.

**Cation-Sensing Properties.** The complexing properties of receptor **4** toward various metal cations ($Li^+$, $Na^+$, $K^+$, $Ca^{2+}$, $Mg^{2+}$, $Ni^{2+}$, $Cu^{2+}$, $Zn^{2+}$, $Cd^{2+}$, $Hg^{2+}$, and $Pb^{2+}$) have been investigated by electrochemistry, spectroscopic measurements, and $^1$H NMR spectroscopy. The results showed that univalent metal cations did not cause significant changes in redox potential, absorption, or the fluorescent emission spectrum, whereas redox shift and remarkable perturbations, both in the absorption and emission spectra, were observed upon the addition of $Hg^{2+}$, $Zn^{2+}$, and $Pb^{2+}$ cations.

Reversibility and relative potentials of redox processes in compound **4** were determined by cyclic (CV) and Osteryoung Square Wave voltammetry (OSWV) in $10^{-3}$ M $CH_3CN$ solutions containing 0.1 M TBAHP as supporting electrolyte. The CV shows two closely spaced reversible one-electron oxidation waves at 0.50 and 0.60 V ($\Delta E_{1/2}$ = 100 mV) respectively for the two ferrocenyl groups. Likewise, the OSWV voltammogram also exhibits two well resolved oxidation peaks at the same potentials. On stepwise addition of $Hg^{2+}$ ions, a clear evolution of the oxidation peaks to 0.56 and 0.65 V ($\Delta E_{1/2}$ = 90 mV) respectively was observed, and maximum perturbation of the OSWV was obtained when 1 equiv of $Hg^{2+}$ cations was added. Receptor **4** also showed perturbation of the oxidation peaks in the presence of $Zn^{2+}$ and $Pb^{2+}$ cations although its behavior is different from that previously observed for $Hg^{2+}$ ions. Thus, upon addition of small amounts of these metal cations a broad oxidation peak, probable due to two overlapped one-electron oxidation peaks, centered at 0.56 and 0.57 V respectively, appeared anodically shifted. The occurrence of these peaks at almost the same potential of the second ferrocene unit suggests that, after oxidation of the first ferrocene unit, the adduct is disrupted and the subsequent oxidation

(42) (a) Barone, V.; Cossi, M. *J. Phys. Chem. A* **1998**, *102*, 1995–2001. (b) Cossi, M.; Rega, N.; Scalmani, G.; Barone, V. *J. Comput. Chem.* **2003**, *24*, 669–681.

(43) (a) Miertus, S.; Scrocco, E.; Tomasi, J. *J. Chem. Phys.* **1981**, *55*, 117–129. (b) Cammi, R.; Mennucci, B.; Tomasi, J. *J. Phys. Chem. A* **2000**, *104*, 5631–5637.

(44) Rinehart, K. L.; Ellis, A. F.; Michejda, C. J.; Kittle, P. A. *J. Am. Chem. Soc.* **1960**, *82*, 4112–4113.

(45) Mueller-Westerhoff, U. T.; Zhou, M. *J. Org. Chem.* **1994**, *59*, 4988–4992.

(46) Rausch, M. D.; Ciappenelli, D. J. *J. Organomet. Chem.* **1967**, *10*, 127–136.

(47) Caballero, A.; Lloveras, V.; Tárraga, A.; Espinosa, A.; Velasco, M. D.; Vidal-Gancedo, J.; Rovira, C.; Wurst, K.; Molina, P.; Veciana, J. *Angew. Chem., Int. Ed.* **2005**, *44*, 1977–1981.

takes place on the partially oxidized $\mathbf{4}^{\bullet+}$. This electrochemically induced complexation/decomplexation process has already been described in some other ferrocene derivatives,[47] and it is associated with a decrease of the association constant when the ligand is oxidized, giving rise to a destabilization of the complex formed. It is worth noting that the different electrochemical responses of **4** toward $Zn^{2+}$ and $Pb^{2+}$ metal ions when compared to $Hg^{2+}$ could indicate a different binding mode exhibited by this ligand in the presence of such metal cations. Remarkably, rotating disk voltammetry studies carried out upon addition of $Cu^{2+}$ to a acetonitrile solution of receptor **4** showed a a significant shift of the sigmoidal voltammetric wave toward cathodic currents, indicating that this metal cation promotes the oxidation of the free receptor (see the Supporting Information). Remarkably, the redox response toward the $Hg^{2+}$ cation is preserved in the presence of an aqueous environment ($CH_3CN/H_2O$ (3/7)) (Figure 1). The presence of $Li^+$, $Na^+$, $K^+$, $Ca^{2+}$, $Mg^{2+}$, $Ni^{2+}$, and $Cd^{2+}$ metal cations had no effect on either the OSWV or CV of the receptor **4**, even when present in large excess.

Previous studies on ferrocene-based ligands have shown that their characteristic low energy (LE) bands in the absorption spectra are perturbed upon complexation.[48] Therefore, the metal recognition properties of the receptor **4** toward the above-mentioned set of metal cations were also evaluated by UV−vis spectroscopy. Titration experiments for $CH_3CN$ solutions of receptor ($c = 1 \times 10^{-4}$ M) and the corresponding metal cations solutions ($c = 2.5 \times 10^{-2}$ M) were performed and analyzed quantitatively.[49] The absorption spectrum of receptor **4** is characterized by a very strong high energy (HE) absoption at 335 nm ($\varepsilon = 10\,970\ M^{-1}\,cm^{-1}$), similar to those reported for pyrido[2,3-*b*]pyrazine derivatives,[50] which is assigned to a localized $\pi-\pi^*$ excitation mainly within the aza-heterocyclic bridge. In addition to this band, another weaker low energy (LE) band is visible at 516 nm ($\varepsilon = 2430\ M^{-1}\,cm^{-1}$) which is assigned to another localized excitation with a lower energy produced by two nearly degenerate transitions, an Fe(II) d−d transition,[51] or a metal-to-ligand charge transfer (MLCT) process ($d_\pi-\pi^*$).[52] Addition of increasing amounts of $Hg^{2+}$ cations to a solution of receptor **4** caused a progressive appearance of a new strong band located at 376 nm ($\varepsilon = 11\,410\ M^{-1}\,cm^{-1}$) and a red shift of the LE band to 628 nm ($\varepsilon = 2890\ M^{-1}\,cm^{-1}$). These changes occur at approximately three well-defined isosbestic points at $\lambda = 351$, 438, and 555 nm, at any receptor/$Hg^{2+}$ ratio, suggesting that only one spectral distinct complex was present. The new LE band is red-shifted by $\Delta\lambda = 112$ nm and is responsible for a perceptible change of color from pale orange to deep green, which can be used for the "naked eye" detection of this divalent cation (Figure 2). Accurate values of the association constant ($K_a$) were determined using standard UV-titration methods. The binding isotherms were generated by recording the changes in the UV absorption as a function of metal cation concentration. Binding assays using the method of continuous variations (Job′s plot) are consistent with a 1:1 binding stoichiometry. The data were well fitted to a 1:1 binding isotherm, and the association constant was calculated: $K_a = 1.1 \times 10^4\ M^{-1}$.

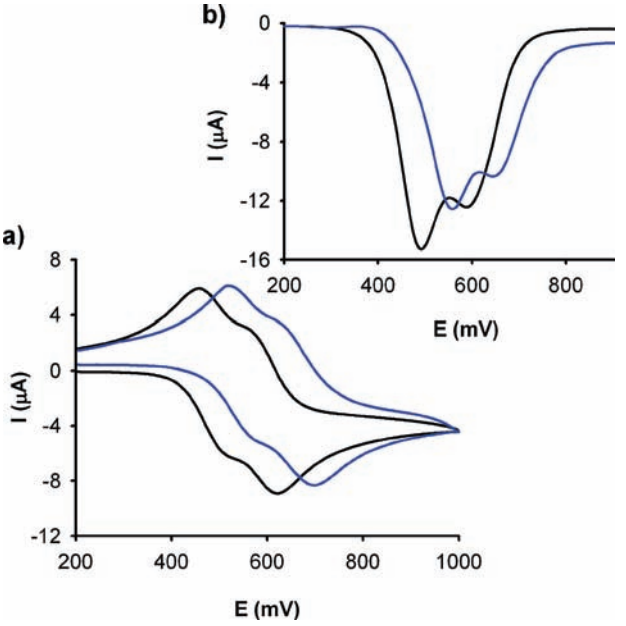


**Figure 1.** (a) CV and (b) OSWV of **4** (0.1 mM) in $CH_3CN/H_2O$ (3/7) $[(n\text{-}Bu)_4N]PF_6$ scanned at 0.1 V $s^{-1}$ before (black) and after (blue) addition of $Hg^{2+}$.

Addition of increasing amounts of $Pb^{2+}$ ions to a solution of the receptor **4** caused a red shift of the low energy band by $\Delta\lambda = 90$ nm, which is responsible from the change of color from pale orange to purple. Three well-defined isosbestic points at 345, 448, and 547 nm indicate that a neat interconversion between the uncomplexed and complexed species occurs. The low energy band of the receptor **4** was also red-shifted ($\Delta\lambda = 42$ nm) upon addition of $Zn^{2+}$ with a concomitant color change from pale orange to purple (Figure 2), and three well-defined isosbestic points at 342, 431, and 337 nm were also observed. Binding assays using the method of continuous variations (Job′s plot) suggests a 2:1 (receptor/metal cation) binding model with a $\beta = 5.42 \times 10^9\ M^{-2}$ for $Pb^{2+}$ and $\beta = 6.5 \times 10^9\ M^{-2}$ for $Zn^{2+}$ cations. By contrast, addition of $Cu^{2+}$ ions to a solution of **4** produces the same perturbation in its absorption spectrum as those observed when **4** was electrochemically oxidized.

Most remarkably is the fact that the colorimetric response toward $Hg^{2+}$ is preserved in the presence of water. Thus, addition of $Hg^{2+}$ cations to a solution of

(48) (a) Marder, S. R.; Perry, J. W.; Tiemann, B. G. *Organometallics* **1991**, *10*, 1896–1901. (b) Coe, B. J.; Jones, C. J.; McCleverty, J. A.; Bloor, D.; Cross, G. J. *J. Organomet. Chem.* **1994**, *464*, 225–232. (c) Müller, T. J.; Netz, A.; Ansorge, M. *Organometallics* **1999**, *18*, 5066–5074. (c) Carr, J. D.; Coles, S. J.; Asan, M. B.; Hurthouse, M. B.; Malik, K. M. A.; Tucker, J. H. R. *J. Chem. Soc., Dalton Trans.* **1999**, 57–62.

(49) Association constants were obtained using the computer program Specfit/32 Global Analysis System, 1994−2004 Spectrum Software Associates (SpecSoft@compuserve.com). The Specfit program was acquired from Biologic SA (www.bio-logic.info) in January 2005.

(50) (a) Thirumurugan, P.; Maralidharan, D.; Rerumal, P. T. *Dyes Pigm.* **2009**, *81*, 245–253. (b) Yamauchi, S.; Hirota, N. *J. Phys. Chem.* **1987**, *91*, 1754–1760.

(51) (a) Geoffroy, G. L.; Wrighton, M. S. *Organometallic Photochemistry*; Academic Press: New York, 1979. (b) Gray, H. B.; Sohn, Y. S.; Hendrickson, N. *J. Am. Chem. Soc.* **1971**, *93*, 3603–3612.

(52) (a) Barlow, S.; Bunting, H. E.; Ringham, C.; Green, J. C.; Bublitz, G. U.; Boxer, S. G.; Perry, J. W.; Marder, S. R. *J. Am. Chem. Soc.* **1999**, *121*, 3715–3723. (b) Southhard, G. E.; Curtis, M. D. *Organometallics* **2001**, *20*, 508–522. (c) Naka, K.; Uemura, T.; Chujo, Y. *Macromolecules* **2000**, *33*, 6965–6969.


**Figure 2.** Changes in the color of receptor **4**, in (a) $CH_3CN$ and (b) $CH_3CN/H_2O$ 3/7, upon addition of the corresponding cation.

receptor **4** in $CH_3CN/H_2O$ (3:7) induced a red shift of the two absorption bands from 345 to 368 nm ($\Delta\lambda$ = 23 nm) and from 539 to 612 nm ($\Delta\lambda$ = 73 nm) ($K_a = 2.51 \times 10^3\ M^{-1}$) (Figure 3). These changes are responsible for the change of color from pale orange to deep green, which can be used for the selective colorimetric detection of $Hg^{2+}$ in aqueous environments, because no changes were observed in the absorption spectrum after addition of either $Pb^{2+}$ or $Zn^{2+}$ cations.

As a complete study of the real application of these metal cations detection, a test paper was prepared by putting a filter paper into the $CH_3CN$ solution of **4** ($2.0 \times 10^{-3}$ M) and then drying it in the air. Clearly, the test paper can detect $Hg^{2+}$, $Pb^{2+}$, and $Zn^{2+}$ from a $CH_3CN$ solution of the metal cations, whereas the other tested ions did not cause any detectable changes (Figure 4).

Receptor **4** exhibits a very weak fluorescence in $CH_3CN$ ($c = 2.5 \times 10^{-5}$ M) the excitation spectrum revealing $\lambda_{exc}$ = 270 nm as an ideal excitation wavelength. The emission spectrum shows a weak and structureless band at 620 nm, with a rather low quantum yield ($\Phi = 2.8 \times 10^{-4}$). Fluorescent titration experiments, by using the same set of metal cations, demonstrate that only $Hg^{2+}$, $Zn^{2+}$, and $Pb^{2+}$ progressively yielded an intense enhancement of the emission band at 620 nm, CHEF (chelation enhancement of fluorescence) = 204 for $Hg^{2+}$, 184 for $Zn^{2+}$, and 90 for $Pb^{2+}$, respectively. The stoichiometry of the complexes was also determined by the changes in the fluorogenic response of receptor **4** in the presence of varying concentrations of these metal cations, and the results indicate the formation of a 1:1 complex for $Hg^{2+}$ and 2:1 complexes for $Zn^{2+}$ and $Pb^{2+}$ cations, with the association constants of $K_a = 2.38 \times 10^4\ M^{-1}$ for $Hg^{2+}$, $\beta = 4.52 \times 10^{10}\ M^{-2}$ for $Zn^{2+}$, and $\beta = 6.73\ 10^{10}$ for $Pb^{2+}\ M^{-2}$. On the other hand, the calculated detection limits were in the range of $10^{-6}$ M. The increase in quantum yield induced by $Hg^{2+}$ ($\Phi$ = 0.013), $Zn^{2+}$ ($\Phi$ = 0.012), and $Pb^{2+}$ ($\Phi$ = 0.005) ions were 46-, 43-, and 18-fold, respectively (Figure 5). When this study was carried out in an aqueous environment ($CH_3CN/H_20$, 3/7) and conducted at pH = 7 (0.1 M HEPES), the emission spectrum of receptor **4** remained unaffected, after addition of the set of metal tested.

The binding stoichiometries proposed from absorption and fluorescent data were further confirmed by electrospray mass spectrometry. The ESI-MS spectrum of receptor **4** in the presence of $Hg^{2+}$ ions displays a peak

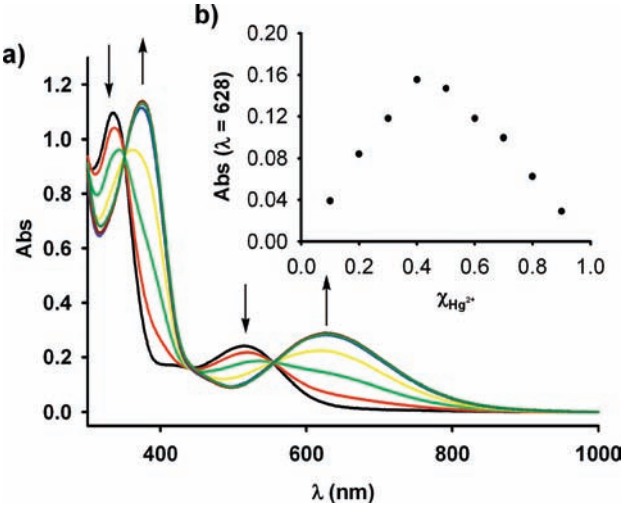


**Figure 3.** (a) Evolution of the UV−vis of **4** (0.1 mM) in $CH_3CN/H_2O$ (3/7) upon addition of increasing amounts of $Hg^{2+}$; arrows indicate the absorptions that increase or decrease during the experiments. (b) Job's plot for **4** and $Hg^{2+}$, indicating the formation of 1:1 (L:M) complex. The total [**4**] + [$Hg^{2+}$] = $1 \times 10^{-4}$M.

at *m*/*z* 701 corresponding to the 1:1 complex although a peak at *m*/*z* 1196 also appears which is probably due to the fragment [**4**-Hg-**4**] resulting from the loss of a Hg ion from a 2:2 complex. In the case of $Pb^{2+}$ ions a peak at *m*/*z* 1305 corresponding to the 2:1 complex is present. This binding stoichiometry is also confirmed for $Zn^{2+}$ ions by the appearance of a peak at *m*/*z* 1062 due to the complex [$\mathbf{4}_2$.$Zn^{2+}$]. The relative abundances of the isotope peak patterns are in each case in good agreement with the corresponding simulated peak patterns.

$^1$H NMR experiments were performed to explore the coordination mechanism of the receptor **4** with the metal cations. In the free receptor, the pyrazine ring creates a nonequivalent magnetic environment for the ferrocenyl units, probably due to the electron withdrawing conjugation effect of the fused pyridine ring. Thus, together with the two different singlets corresponding to the unsubstituted Cp rings belonging to both ferrocene subunits, three sets of signals associated to the two monosubstituted Cp rings are also observed: two overlapped pseudotriplets due to the $H_\beta$ and $H_{\beta'}$ protons ($\delta$ = 4.35 ppm) and two separated pseudotriplets ($\delta$ = 4.68 and $\delta$ = 4.77 ppm) assigned to the $H_\alpha$ and $H_{\alpha'}$ protons. In addition, compound **4** also exhibits three double doublets attributed to the H-6 ($\delta$ = 9.05 ppm, $J$ = 4.2 Hz and $J$ = 1.8 Hz), H-7 ($\delta$ = 7.59 ppm, $J$ = 8.4 Hz and $J$ = 4.2 Hz), and H-8 ($\delta$ = 8.35 ppm, $J$ = 8.4 Hz and $J$ = 1.8 Hz) present in the heterocyclic system (Table 1). The spectra of the complexes are characterized by a deshielding of the pyridine protons with reference to the free receptor. This change in the proton environment upon coordination results from a decrease in electron density induced by the positive metal cation center. For all complexes only one set of aromatic signals (three double−doublets) was found, showing that highly symmetrical compounds were formed.

Regarding the ferrocene signals, the most remarkable feature is the strong chemical shift change observed for the signals associated with one ferrocene unit. The unsubstituted cyclopentadienyl protons move by ca. $\Delta\delta$ −0.53 ppm, and the monosubstituted ring protons

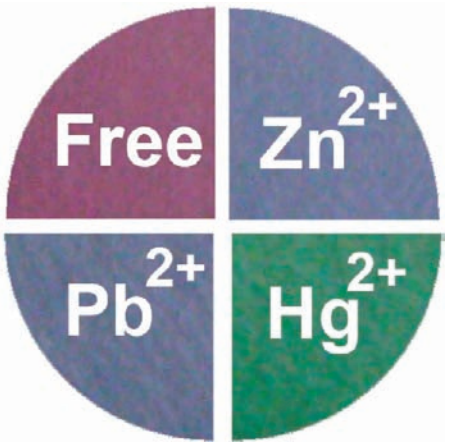


**Figure 4.** Changes in the color of the test papers based on **4**, for detecting $Hg^{2+}$, $Pb^{2+}$, and $Zn^{2+}$ in a $CH_3CN$ solution.

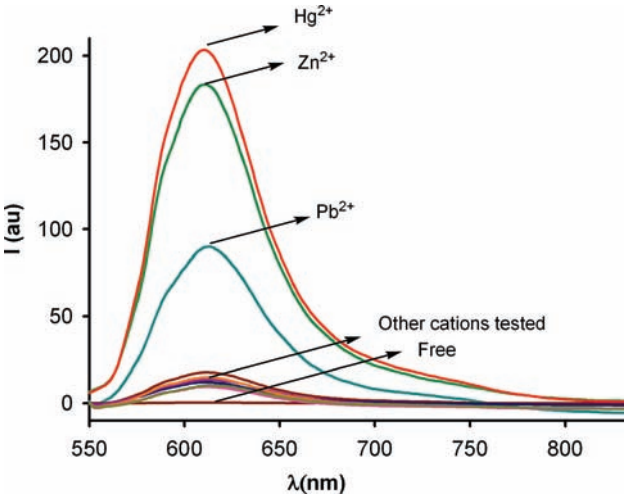


**Figure 5.** Fluorescence spectra of **4** ($1 \times 10^{-5}$ M in $CH_3CN$) in the presence of several cations ($\lambda_{exc}$ = 270 nm).

are also upshifted by $\Delta\delta$ −0.44 ppm on complexation with $Zn^{2+}$ ions (Figure 6), as a result of the anisotropic shielding effects exerted upon them by the heteroaromatic unit (see below).

Data collected in Table 1 suggest different bridging coordination modes. Thus, upon complexation with $Pb^{2+}$ cations the pyridine H-8 proton underwent the largest downfield shift $\Delta\delta_{H\text{-}8}$ = +0.51 ppm, whereas the H-6 proton is the lowest downshift $\Delta\delta_{H\text{-}6}$ = +0.02 ppm. In addition, the difference in chemical shifts between H-6 and H-8 is 0.21 ppm, considerably lower than values found not only in the free receptor (0.70 ppm) but also in complexes with $Zn^{2+}$ (0.56 ppm) and $Hg^{2+}$ (0.54 ppm) cations. By contrast, the H-6 proton is further downshifted ($\Delta\delta_{H\text{-}6}$ = +0.19−0.12 ppm) and the H-8 proton is shifted less ($\Delta\delta_{H\text{-}8}$ = +0.33−0.28 ppm) upon complexation with $Zn^{2+}$ or $Hg^{2+}$ than with $Pb^{2+}$ cations, which means that the N-5 of the pyridine ring could be involved in the complexation process. Taking into account the 1:1 stoichiometry of the complex with $Hg^{2+}$, deduced from spectroscopic and spectrometric data, as well as the broad signals in the $^1H$ NMR spectrum, participation of N-4 and N-5 (exobidentate ligand) in the complex formation is not discarded.[53] Titration isotherms, generated from the change in chemical shift of the $H_7$ signal upon addition of $Hg^{2+}$, $Zn^{2+}$, and $Pb^{2+}$ cations, confirmed the stoichiometries of the complexes formed, using the computer program EQNMR.[54] The derived association constants were $K_a = 9.1 \times 10^3$ $M^{-1}$, for $Hg^{2+}$; $\beta = 9.1 \times 10^8$ $M^{-2}$, for $Zn^{2+}$; and $\beta = 9.3 \times 10^8$ $M^{-2}$, for $Pb^{2+}$ (error < 10%).

The coordination modes of receptor **4** toward divalent metal cations $Zn^{2+}$, $Hg^{2+}$, and $Pb^{2+}$ have also been studied with the aid of quantum chemical calculations. Pure electrostatic arguments based, for instance, on atomic natural charges[55] would point to N5 in the pyridine ring of **4** as more basic (−0.496 au) than pyrazine N4 (−0.445 au) and N1 (−0.432 au) atoms, in agreement with the expected higher electron density on the pyridine ring over the pyrazine (−0.624 and −0.131 au, respectively, extended over all ring heavy atoms). Similarly Mulliken charges predict higher pyridine vs pyridazine electron density (−0.380 au vs −0.256 au) although a different basicity sequence is obtained: N1 (−0.493 au) ≥ N5 (−0.487 au) > N4 (−0.437 au). Finally, steric crowding at N1 and N4, due to the proximity of the ferrocenyl substituents, could be invoked to select, in principle, N5 as the best donor candidate.

The preference among several donor atoms to interact with an acidic center can also be qualitatively analyzed in the context of Pearson's hard−soft acid−base (HSAB) principle.[56] During the past two decades many important concepts and parameters related to chemical reactivity have been rationalized within the framework of DFT.[57] The DFT formulation of the HSAB principle[58] states that the most favorable situation occurs when the reactants have equal softness provided that the charge reshuffling step can be neglected. The best suited *local* reactivity index for studying regioselectivity[59] is local softness $s(\mathbf{r})$, easily obtained from the Fukui function $f(\mathbf{r})$, defined by Parr and Yang,[60] and the global softness $S = (\partial N/\partial\mu)_{v(\mathbf{r})}$, which describes the ability of the molecule to take or lose electrons in response to a change in the chemical potential, $\mu$. Therefore $s(\mathbf{r})$ describes both the charge transfer between the reactants and how charge is redistributed within the reactants themselves. A local HSAB principle can then be devised as follows: a regioisomer is favored when the new bond is formed between atoms of equal

(53) (a) Wan, Y.; Niu, W.; Behof, W. J.; Wang, Y.; Boyle, P.; Gorman, C. B. *Tetrahedron* **2009**, *65*, 4293–4297. (b) van den Ancker, T. R.; Engelhardt, L. M.; Henderson, M. J.; Jacobsen, G. E.; Raston, C. L.; Skelton, B. W.; White, A. H. *J. Organomet. Chem.* **2004**, *689*, 1991–1999.

(54) Haynes, M. J. *J. Chem. Soc., Dalton Trans.* **1993**, 311–312.

(55) (a) Carpenter, J. E.; Weinhold, F. *THEOCHEM* **1988**, *169*, 41–62. (b) Carpenter, J. E. Ph.D. thesis, University of Wisconsin, Madison, WI, **1987**. (c) Foster, J. P.; Weinhold, F. *J. Am. Chem. Soc.* **1980**, *102*, 7211–7218. (d) Reed, A. E.; Weinhold, F. *J. Chem. Phys.* **1983**, *78*, 4066–4073. (e) Reed, A. E.; Weinstock, R. B.; Weinhold, F. *J. Chem. Phys.* **1985**, *83*, 735–746. (f) Reed, A. E.; Curtiss, L. A.; Weinhold, F. *Chem. Rev.* **1988**, *88*, 899–926.

(56) Pearson, R. G. *J. Am. Chem. Soc.* **1963**, *85*, 3533–3539.

(57) Parr, R. G.; Yang, W. *Density Functional Theory of Atoms and Molecules*; Oxford University Press: Oxford, 1989.

(58) (a) Chattaraj, P. K.; Lee, H.; Parr, R. G. *J. Am. Chem. Soc.* **1991**, *113*, 1855–1856. (b) Cedillo, A.; Chattaraj, P. K.; Parr, R. G. *Int. J. Quantum Chem.* **2000**, *77*, 403–407.

(59) See for instance: Ponti, A.; Molteni, G. *Chem.—Eur. J.* **2006**, *12*, 1156−1161 and references cited therein.

(60) Parr, R. G.; Yang, W. *J. Am. Chem. Soc.* **1984**, *106*, 4049–4050.

**Table 1.** Significant $^1$H NMR Changes Observed during the Recognition Processes[a]

| | $H_6$ ($\Delta\delta$) | $H_7$ ($\Delta\delta$) | $H_8$ ($\Delta\delta$) | $H_{\alpha'}$ ($\Delta\delta$) | $H_{\alpha}$ ($\Delta\delta$) | $H_{\beta'}$ ($\Delta\delta$) | $H_{\beta}$ ($\Delta\delta$) | Cp(2) ($\Delta\delta$) | Cp(3) ($\Delta\delta$) |
|---|---|---|---|---|---|---|---|---|---|
| **4** | 9.05 | 7.59 | 8.35 | 4.77 | 4.68 | 4.35 | 4.35 | 4.10 | 4.30 |
| **4**·$Zn^{2+}$ | 9.24 | 7.99 | 8.68 | 4.33 | 4.59 | 4.36 | 4.36 | 4.12 | 3.77 |
| | (+0.19) | (+0.4) | (+0.33) | (−0.44) | (−0.09) | (+0.01) | (+0.01) | (+0.02) | (−0.53) |
| **4**·$Pb^{2+}$ | 9.07 | 7.95 | 8.86 | 4.86 | 4.76 | 4.61 | 4.46 | 4.04 | 3.97 |
| | (+0.02) | (+0.36) | (+0.51) | (+0.09) | (+0.08) | (+0.26) | (+0.11) | (−0.06) | (−0.33) |
| **4**·$Hg^{2+}$ | 9.17 | 7.88 | 8.63 | 4.92 | 4.92 | 4.58 | 4.58 | 4.19 | 4.19 |
| | (+0.12) | (+0.29) | (+0.28) | (+0.15) | (+0.24) | (+0.23) | (+0.23) | (+0.09) | (−0.11) |

[a] $H_\alpha$, $H_\beta$, and Cp2 are used to designate the H atoms within the mono- and unsubstituted cyclopentadenyl units present in the ferrocene moiety linked to the C-2 in the heterocyclic ring, while $H_{\alpha'}$, $H_{\beta'}$, and Cp3 designate the same group of atoms in the ferrocene linked to C-3.

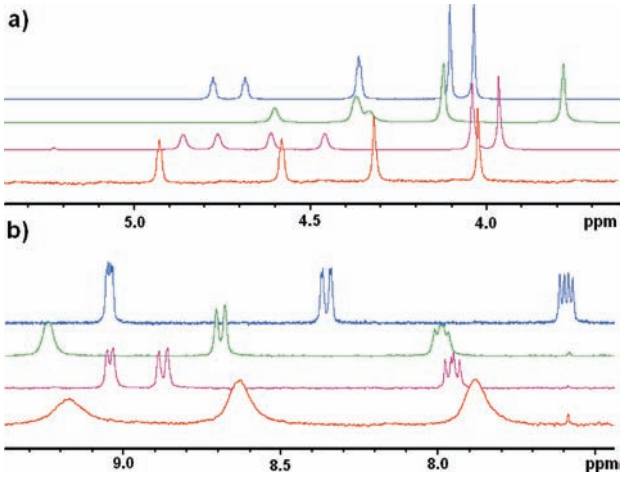


**Figure 6.** $^1$H NMR spectral changes observed in **4** (blue) in $CD_3CN$, after the addition of 0.5 equiv of $Zn^{2+}$ (green), 0.5 equiv of $Pb^{2+}$ (purple), or 1 equiv of $Hg^{2+}$: (a) ferrocene protons and (b) pyridine protons.

softness. In other words, the preferred regioisomer in the reaction between atom $k$ in molecule A and molecule B will be formed on reaction at atom $l$ that minimizes the quadratic difference in local condensed-to-atom softness function[61] $\Delta(s^2)_{kl} = (s_{Ak} - s_{Bl})^2$. An analogous parameter $\Delta(\omega^2)_{kl} = (\omega_{Ak} - \omega_{Bl})^2$ has been proposed,[62] based on local philicities $\omega(\mathbf{r})$ which, in turn, can be easily calculated, *via* Fukui functions $f(\mathbf{r})$, from the global philicity[63] $\omega = \mu^2 S$, measuring the stabilization in energy when the system acquires an additional electronic charge, $\Delta N$, from the environment. For situations in which condensed local softness was found inadequate to provide the correct intermolecular reactivity trends, the group softness[64] descriptor, $s_{(k)g}$, and group philicity,[65] $\omega_{(k)g}$, descriptors have been highlighted, which are obtained after summing the condensed local property—softness or philicity—over all of the $n$ neighboring atoms attached to the reactive site $k$. Finally, in the very first step of the bond-forming interaction between atoms $k$ and $l$, charge is transferred within them, equalizing the electron chemical potential and inducing a variation of the grand potential $\Delta\Omega$ of the system. The contribution due to the interaction of atoms $k$ and $l$ is $\Delta\Omega_{kl} = -^1/_2(\mu_A - \mu_B)^2 s_{Ak} s_{Bl}/(s_{Ak} + s_{Bl})$. Table 2 collects the values for all three parameters $\Delta(s^2)_{kl}$, $\Delta(\omega^2)_{kl}$, and $\Delta\Omega_{kl}$ computed for the basic attack of all three possible N donor atoms in ligand **4** to the metal center in the corresponding diperchlorate salts.[66] These data unambiguously demonstrate the preference of the attack of **4** through its N5 donor atom to $Zn^{2+}$, $Hg^{2+}$, or $Pb^{2+}$. Furthemore, the above-mentioned kinetic preference was also found to parallel the calculated thermodynamic stability of the hypothetical resulting 1:1 (ligand/metal) complexes (Table 2). Thus, adducts resulting from N4- or N5-complexation were found to yield the same N4,N5-chelates (herein named as N45 binding modes, for short) which displayed higher stability than the N1-coordination isomers. At least part of the destabilization of the N1-complexation products may arise from their higher ligand strains (Table 2) originated by the sterically demanding adjacent ferrocenyl group.

The structures for the actual complexation species have been computed taking into account the experimentally observed ligand-to-metal stoichiometries and after thorough check of all conceivable binding modes and conformations. Thus, the most stable 2:1 complex with a $Zn^{2+}$ cation was found to display the aforementioned N45 coordination in one of the ligands ($d_{N5-Zn}$ = 2.198 Å, $d_{N4-Zn}$ = 2.414 Å; $WBI_{N5-Zn}$ = 0.106, $WBI_{N4-Zn}$ = 0.066), but an almost pure N5 binding mode for the other one ($d_{N5-Zn}$ = 2.127 Å, $d_{N4-Zn}$ = 2.877 Å; $WBI_{N5-Zn}$ = 0.116, $WBI_{N4-Zn}$ = 0.030), presumably due to steric crowding around the relatively small metal ion (Figure 7). Both ligands in $\mathbf{4}_2 \cdot Zn(ClO_4)_2$ are expected to reach a fluxional equilibrium in solution that exchanges their binding roles. Three perchlorate O atoms complete the first coordination sphere around the metal. Worthy of mention is that the N45 bound ligand locates its C3-linked ferrocenyl group above the pyridine ring belonging to the N5 bound ligand. The resulting T-stacking of the unsubstituted Cp H atoms over the heterocyclic ring ($d_{H\ldots ring}$ = 2.747 Å, $WBI_{H\ldots ring}$ = 0.003) would explain the unexpected large upfield shift observed for one of the Cp signals in the H NMR spectrum on complexation (Figure 6a). Furthermore, the position of this ferrocene group is relatively fixed by

(61) (a) Damoun, S.; Van deWoude, G.; Méndez, F.; Geerlings, P. *J. Chem. Phys.* **1997**, *101*, 886–893. (b) Ponti, A. *J. Phys. Chem. A* **2000**, *104*, 8843–8846.

(62) Espinosa, A.; Frontera, A.; García, R.; Soler, M. A.; Tárraga, A. *Arkivoc* **2005**, *ix*, 415–437.

(63) Parr, R. G.; Szentpaly, L. V.; Liu, S. *J. Am. Chem. Soc.* **1999**, *121*, 1922–1924.

(64) (a) De Proft, F.; Langenaeker, W.; Geerlings, P. *J. Phys. Chem.* **1993**, *97*, 1826–1831. (b) De Proft, F.; Amira, S.; Choho, K.; Geerlings, P. *J. Phys. Chem.* **1994**, *98*, 5227–5233. (c) Kishnamurty, S.; Pal, S. *J. Phys. Chem. A* **2000**, *104*, 7639–7645.

(65) Parthasarathi, R.; Padmanabhan, J.; Elango, M.; Subramanian, V.; Chattaraj, P. K. *Chem. Phys. Lett.* **2004**, *394*, 225–230.

(66) In the case of the large $Pb^{2+}$ cation we have used a $[Pb(ClO_4)_2(CH_3CN)_2]$ species as a model for the complexating reagent.

**Table 2.** Relevant HSAB-Related Calculated Parameters[a] for the Reaction of N-Donor Atoms in Ligand **4** with Metal Diperchlorates and Complexation Energies for the Resulting 1:1 Complexes

| | Zn | Hg | Pb[b] |
|---|---|---|---|
| $\Delta(s^2)_{kl}$ [c,d] | 5.2/5.2/4.4 | 16.7/16.8/15.3 | 4.0/4.0/3.3 |
| $\Delta(\omega^2)_{kl} \times 10^2$ [c,d] | 1.2/1.2/1.2 | 3.6/3.6/3.5 | 5.1/5.1/4.7 |
| $\Delta\Omega_{kl}$ [c,e] | 1.9/1.9/1.3 | 2.1/2.0/1.4 | 0.8/0.8/0.5 |
| $\Delta E_{compl}$ [e,f] | −63.5/−124.1 | −45.7/−55.2 | 2.8/−46.3 |
| $L_{strain}$ [e,f] | 14.4/11.6 | 45.6/9.6 | 16.8/7.4 |

[a] Derived from natural charges. [b] See text. [c] N1/N4/N5 ratio. [d] Group property. [e] kJ·mol$^{-1}$. [f] N1/N45 ratio.

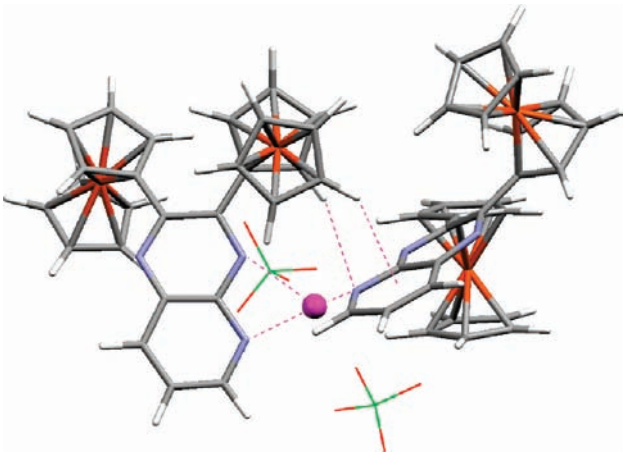

**Figure 7.** Calculated structure for the $\mathbf{4}_2 \cdot Zn(ClO_4)_2$ complex. Perchlorate ligands are displayed in wireframe for clarity.

addidional hydrogen bonding between a $H_\alpha$ atom in the monosubstituted Cp ring and the pyrazine N4 atom ($d_{H\ldots N4}$ = 2.648 Å, $WBI_{H\ldots N4}$ = 0.007). Bader's AIM methodology allows convenient characterization of these subtle interactions by identification of the corresponding BCPs (bond critical points), the extent of the interaction being correlated with the electron density and its Laplacian at the BCP, in this case $\rho(r_{c[H\ldots N4]}) = 0.75 \times 10^{-2}$ e/$a_0{}^3$ and $\nabla^2 \rho(r_{c[H\ldots N4]}) = 2.21 \times 10^{-2}$ e/$a_0{}^5$, respectively.

Ligand **4** behaves similarly in the reaction with $Pb(ClO_4)_2$, although in this case the large $Pb^{2+}$ cation allows the approximation of two ligands exhibiting N45 binding behavior ($d_{N5\ldots Pb}$ = 2.546 and 2.864 Å, $WBI_{N5\ldots Pb}$ = 0.170 and 0.108; $d_{N4\ldots Pb}$ = 2.769 and 2.747 Å, $WBI_{N4\ldots Pb}$ = 0.118 and 0.139) in the most stable 2:1 complex $\mathbf{4}_2 \cdot Pb(ClO_4)_2$ with two very similar heterocyclic ligands (Figure 8), whose largest difference deals with the alternated/eclipsed conformations of the ferrocenyl groups at C-2.

In the case of $Hg^{2+}$, the most likely structure is that of the above-mentioned 1:1 complex exhibiting typical N−Hg bond distances ($d_{N5\ldots Hg}$ = 2.491 Å, $WBI_{N5\ldots Hg}$ = 0.147; $d_{N4\ldots Hg}$ = 2.518 Å, $WBI_{N4\ldots Hg}$ = 0.124) (Figure 9).

It is worth mentioning that this metal cation displays the smallest difference in complexation energy between the N45 and N1 binding modes (Table 2) in comparison to $Zn^{2+}$ and $Pb^{2+}$.

We have obtained the optimized structure for the complexation product between a free terminal N1 atom in the most stable 1:1 complex $\mathbf{4} \cdot Hg(ClO_4)_2$, involving the N45 coordination mode, with an additional identical molecule

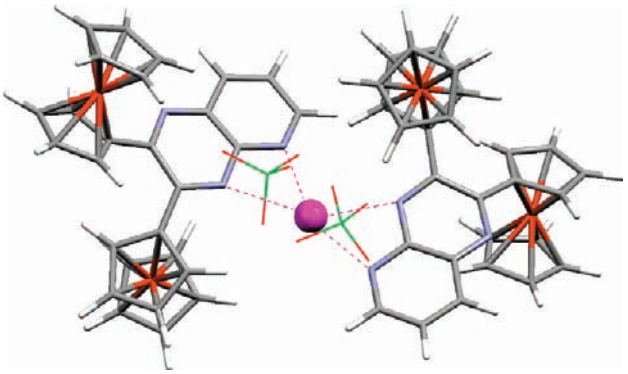

**Figure 8.** Calculated structure for the $\mathbf{4}_2 \cdot Pb(ClO_4)_2$ complex. Perchlorate ligands are displayed in wireframe for clarity.

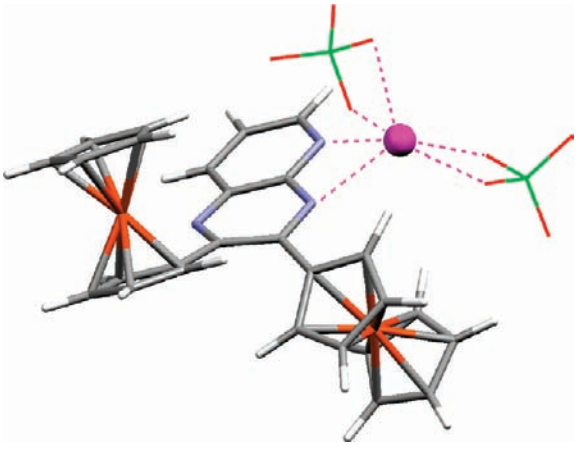

**Figure 9.** Calculated structure for the $\mathbf{4} \cdot Hg(ClO_4)_2$ complex. Perchlorate ligands are displayed in wireframe for clarity.

(Figure 10), i.e. a 2:2 complex. In addition to the N−Hg bonds in the internal ($d_{N5\ldots Hg}$ = 2.477 Å, $WBI_{N5\ldots Hg}$ = 0.143; $d_{N4\ldots Hg}$ = 2.618 Å, $WBI_{N4\ldots Hg}$ = 0.102; $d_{N1\ldots Hg}$ = 2.484 Å, $WBI_{N1\ldots Hg}$ = 0.127) and peripheral linkages ($d_{N5\ldots Hg}$ = 2.506 Å, $WBI_{N5\ldots Hg}$ = 0.135; $d_{N4\ldots Hg}$ = 2.485 Å, $WBI_{N4\ldots Hg}$ = 0.127), the most prominent structural feature in this complex is the significant interaction of the internal $Hg^{2+}$ cation with an adjacent ferrocenyl iron atom ($d_{Fe\ldots Hg}$ = 3.031 Å, $WBI_{Fe\ldots Hg}$ = 0.155; $\rho(r_{c[Fe\ldots Hg]}) = 2.39 \times 10^{-2}$ e/$a_0{}^3$; $\nabla^2 \rho(r_{c[Fe\ldots Hg]}) = 4.89 \times 10^{-2}$ e/$a_0{}^5$). This latter interaction could be responsible for the most pronounced color change of the ligand on complexation to $Hg^{2+}$ cations when compared to the other metal ions for which such an additional binding mode was not observed. Indeed, the MO diagrams for the ligand **4** and its complexes (see the Supporting Information) clearly show that the optical transitions should occur between the ferrocene-centered HOMOs and the $\pi^*$-type LUMOs, located on the heterocyclic moieties, and that the HOMO−LUMO gap decreases on complexation, this effect being more pronounced for the case of the mercury 2:2 complex.

An alternative 2:2 discrete arrangement locating two Hg atoms in the inner cavity between two antiparallel ligands oriented with the N4 and N5 atoms inward was ruled out by energetic considerations.

It is also worth noting that the $Hg^{2+}$ cation does not promote oxidation of the ligands at the electroactive ferro-

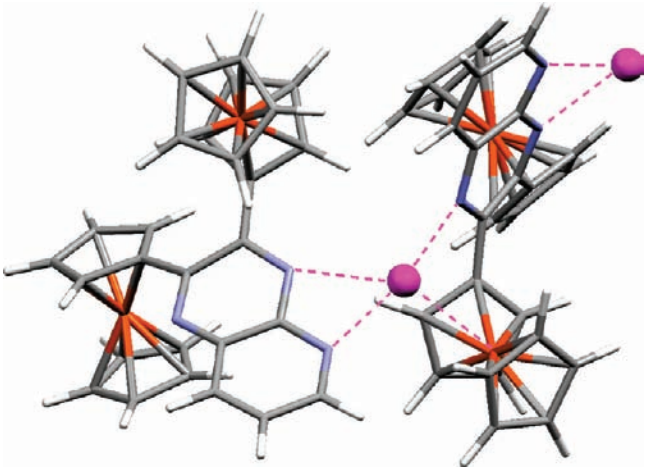

**Figure 10.** Calculated structure for the mercury 2:2 complex. Perchlorate ligands are omitted for clarity.

cenyl groups as previously observed in other ferrocenyl-substituted mercury(II) complexes.[25c] This fact is evidenced by the small distortion of the highly sensitive distance between the Fe atom and the unsubstituted Cp ring centroid in all four ferrocenyl groups at either the 1:1 complex $\mathbf{4}\cdot Hg(ClO_4)_2$ ($\Delta d = 0.57 \times 10^{-2}$ and $0.09 \times 10^{-2}$ Å) or the 2:2 complex ($\Delta d = 5.18 \times 10^{-2}$, $4.38 \times 10^{-2}$, $1.52 \times 10^{-2}$, $0.94 \times 10^{-2}$, $0.99 \times 10^{-2}$, $0.78 \times 10^{-2}$, and $0.4909 \times 10^{-2}$ Å) of the complex when compared in relation to those in the free ligand (average 1.618 Å)[67] Obviously the largest distortion corresponds to the ferrocenyl group interacting with the N1-bound internal $Hg^{2+}$ cation in the dimeric species and is therefore not attributable to any internal redox process, as it displays a remarkable inter-Cp tilt angle ($\beta = 15.63°$) not observed in ferrocenium units.[68]

(67) The computed distortion for the mono-oxidized derivatives of 2- and 3-ferrocenyl analogues of ligand **4** are $5.08 \times 10^{-2}$ and $5.22 \times 10^{-2}$ Å, respectively, whereas the monooxidized diferrocenyl ligand $\mathbf{4}^{\bullet+}$ exhibits halfway distortion ($3.08 \times 10^{-2}$ and $3.48 \times 10^{-2}$ Å) at every half-oxidized ferrocene unit.

(68) (a) Caballero, A.; García, R.; Espinosa, A.; Tárraga, A.; Molina, P. *J. Org. Chem.* **2007**, *72*, 1161–1173. (b) Small $\beta$ tilt angles (defined as the complementary of the $Cp^{\#}-Fe-Cp^{\#}$ angle, $Cp^{\#}$ standing for the Cp ring centroids) are obsrerved for the mono-oxidized 2- and 3-ferrocenyl analogues of ligand 4 (1.40° and 1.26°, respectively), as well as for the Fc groups of $4^{\cdot+}$ (0.66° and 0.78°).

## Conclusion

We have prepared a member of a potential class of easy-to-synthesize ferrocene-based azaquinoxaline receptors and examined its binding properties toward various guest cations by using electrochemical, spectral, and optical techniques as well as DFT-based quantum chemical calculations. Our synthetic methodology is based on the improved preparation of the not readily available diferrocenylethane-1,2-dione and subsequent condensation with 2,3-diaminopyridine.

Receptor **4** displays, in $CH_3CN$ solution, the same type of sensing properties toward $Hg^{2+}$, $Pb^{2+}$, and $Zn^{2+}$ metal cations: the oxidation redox peak is anodically shifted, and a highly fluorescence enhancement ( > 90-fold) in conjunction with a visible colorimetric change can be observed. Remarkably, the redox and colorimetric responses toward $Hg^{2+}$ cations are preserved in the presence of water ($CH_3CN/H_2O$, 3/7). Significantly, receptor **4** represents a rare example in which the redox and the convenient "naked-eye" and fluorescent $Hg^{2+}$ detection are possible with a single molecule.

Moreover, dyad **4** also exhibited a selective $Pb^{2+}$ and $Zn^{2+}$ metal cation redox induced complexation/decomplexation type of signaling patterns.

**Acknowledgment.** We gratefully acknowledge the financial support from MICINN-Spain, Project CTQ2008-01402 and Fundación Séneca (Agencia de Ciencia y Tecnología de la Región de Murcia) project 04509/GERM/06 (Programa de Ayudas a Grupos de Excelencia de la Región de Murcia, Plan Regional de Ciencia y Tecnología 2007/2010). A.C. also thanks the Ministerio de Educación y Ciencia for a predoctoral grant.

**Supporting Information Available:** Electrochemical, NMR, UV−vis, and emission spectral data. Detection limit calculations. Calculated structures. This material is available free of charge via the Internet at http://pubs.acs.org.